Auton Robot (2015) 39:25–41
DOI 10.1007/s10514-015-9425-4

Finger contact sensing and the application in dexterous hand manipulation

Hongbin Liu · Kien Cuong Nguyen · Véronique Perdereau · Joao Bimbo · Junghwan Back · Matthew Godden · Lakmal D. Seneviratne · Kaspar Althoefer

Received: 11 March 2013 / Accepted: 3 January 2015 / Published online: 21 January 2015

Abstract In this paper we introduce a novel contact-sensing algorithm for a robotic fingertip which is equipped with a 6-axis force/torque sensor and covered with a deformable rubber skin. The design and the sensing algorithm of the fingertip for effective contact information identification are introduced. Validation tests show that the contact sensing fingertip can estimate contact information, including the contact location on the fingertip, the direction and the magnitude of the friction and normal forces, the local torque generated at the surface, at high speed (158–242 Hz) and with high precision. Experiments show that the proposed algorithm is robust and accurate when the friction coefficient ≤ 1. Obtaining such contact information in real-time are essential for fine object manipulation. Using the contact sensing fingertip for surface exploration has been demonstrated, indicating the advantage gained by using the identified contact information from the proposed contact-sensing method.

Keywords Contact sensing for deformable fingertip · Tactile sensing · Surface following control

H. Liu (✉) · J. Bimbo · J. Back · L. D. Seneviratne · K. Althoefer
Department of Informatics, Centre for Robotics Research, King's College London, London, UK
e-mail: hongbin.liu@kcl.ac.uk

K. C. Nguyen · V. Perdereau
Université Pierre et Marie Curie, Paris 6, France

M. Godden
Shadow Robot Company, London, UK

L. D. Seneviratne
Khalifa University, Abu Dhabi, United Arab Emirates

1 Introduction

Despite the success of robotic manipulation devices when operating in static and well structured environments such as factories, today's most advanced robots still struggle to perform simple manipulation tasks which are trivial to a human outside a controlled environment (Kemp et al. 2007). Robots that are capable of replacing humans in conducting manipulation tasks are increasingly demanded in operations carried out in unstructured remote and hazardous environments. Human are very efficient in manipulation tasks largely due to sophisticated tactile sensing mechanisms distributed across the human hand. Neurophysiology studies show that when humans manipulate objects, the tactile afferents of the hand provide the brain with comprehensive information related to the contact, such as the contact locations, the spatial distribution, the direction and magnitude of contact forces, surface texture and the local shape of the contacted surface (Johansson and Flanagan 2009). Such information permits humans to be extremely proficient in manipulating and recognizing object based on the sense of touch alone (Lederman and Klatzky 1990). Another study (Rothwell et al. 1982) reveals that persons with neurological damage to tactile sensing system of their hand cannot perform fine manipulation tasks such as fastening a button or using a pen to write.

As it is the case for human, in order to for a robot to perform manipulation tasks efficiently, the precise and real-time identification of the contact information between the finger(s) and the object is essential (Bicchi 2000). It is noted that most developed theories for object grasping and manipulation require an accurate estimation of finger-object interaction such as contact locations, and normal and tangential force (Kao and Cutkosky 1993; Howe and Cutkosky 1996). In addition, the accurate estimation of contact information is vital to allow a robotic hand to recognize the attributes of

an object which can only to be rendered through touch, as surface texture (Jamali and Sammut 2011; Liu et al. 2012a), fine surface features (Okamura and Cutkosky 2001), object shape and poses (Liu et al. 2012b; Bimbo et al. 2013). A human's contact sensing capability is still far beyond that of robots hitherto. To narrow the gap, extensive research has been carried out to date. A lot of effort has been put into the development of tactile skins consisting of distributed tactile sensing elements. Different technologies have been investigated to develop tactile skins with uniaxial pressure sensing capability including a range of tactile array sensors made of conductive rubber (Shimojo et al. 2004; Teshigawara et al. 2011), capacitive materials (Salo et al. 2006; Schmitz et al. 2011), piezo-resistive material (Wisitsoraat et al. 2007), piezoelectric material (Dargahi 2000; Dahiya et al. 2011), and optical fibres (Puangmali et al. 2012). Extensive surveys on the developments of tactile skins are provided in (Yousef et al. 2011; Dahiya et al. 2010). To provide shear force sensing ability, tactile skins that can measure distributed multi-dimensional contact forces have also been developed in recent years. An optical three axis tactile sensor which can measure shear and normal forces was developed by Ohka et al. (2008) using a CCD camera and an array of rubber nodes. A fingertip sensor that consists of a weakly conductive fluid and multiple electrodes was proposed by Wettels et al. (2008) and later commercialized as the BioTac fingertip by SynTouch. This sensor can measure three axial contact forces, vibrations and temperature. The use of optoelectronic components for constructing a tactile sensor has been proposed by De Maria et al. (2012). This sensor can provide both spatial pressure distribution and 6-axis force/torque information. The current bottleneck for developing tactile skin consisting of distributed tactile sensing elements is that it is a trade-off between the spatial resolutions of the sensing elements and design complexity.

Another approach to determine the contact information on an end-effector is to use force/torque sensors. This type of sensor can be used to perceive the interaction forces and detect the occurrence of object slip (Ho et al. 2011) and can also be used for identifying the contact locations based on the dynamic modelling of object-hand interaction (Salisbury 1984). The "intrinsic contact sensing" method, in which the three dimensional contact location and local torque are estimated using force/torque measurements, was proposed by Bicchi et al. (1993). This method has been applied for contact sensing of the feet in a pipe crawling robot (Gálvez and Gonzalez de Santos 2001), for identifying the surface shape properties using a robot fingertip (Murakami and Hasegawa 2005; Yamada et al. 2010). In our previous works, it has also been used for surface material recognition (Liu et al. 2012a, b), slip prediction (Song et al. 2012, 2014) and surface contour tracking (Back et al. 2014) using rigid fingertips. The limitation of the intrinsic sensing method proposed in (Bicchi et al. 1993) is that it is strictly constrained to low friction contacts and the rigid contact surface is assumed without considering soft finger deformation. In addition, the method assumes a single contact location. When there are multiple contacts, the algorithm provides one contact location that is resultant estimation of the multiple contacts. A number of approaches for studying the relationship between the external contact force and the geometrical deformation of a soft finger have been proposed in the literature. Xydas and Kao (1999) extended the Hertzian contact model and proposed a power law contact model based on continuum mechanics theory. The coefficient of this model was later experimentally identified in (Kao and Yang 2004). The limitation of the continuum mechanics theory is the infinitesimal elastic deformation assumption which is often violated for soft finger contact. Inoue and Hirai (2006, 2009) proposed the concept of "virtual spring" which assumes that the soft body is composed of infinite and unconnected linear springs to counterbalance the external load. This method can practically model a soft finger undergoing considerable large deformation with a good accuracy. A similar approach has also been implemented in (De Maria et al. 2013) for modelling the tactile response of a soft fingertip sensor. In this paper, we propose an improved fingertip intrinsic contact sensing algorithm based on 6-axis force/torque measurements, by integrating the mechanical model of a deformable skin. The contact information to be estimated includes the contact location on the fingertip, the direction and the magnitude of the friction and normal forces, the local torque generated at the surface and the surface deformation. Compared to the use of tactile array fingertip sensing, the advantage of the proposed approach is that it could provide both higher spatial resolution of the contact location and more accurate three dimensional interaction forces/torques information of the contact. Furthermore, only the fingertip only requires a single force/torque sensor which is relative easy to be manufactured. In addition, as human manipulating objects, there is often only one contact area per fingertip. Hence the constraint of single contact location on the fingertip of the selected approach is expected to be satisfied in most manipulation tasks. Since the deformable skin on a fingertip is often subjected to notable local deformation, the "virtual spring" method is adopted for the rubber skin mechanical modelling. The incompressibility of elastic material is not considered by using the "virtual spring" modelling method. Compared to the intrinsic sensing algorithm proposed in (Bicchi et al. 1993), the novelty of the contact sensing algorithm proposed in this paper is twofold: (1) capability of estimating the contact location with a deformable finger skin, by taking into account the relationship between the contact normal force and surface deformation, (2) relaxation of the constraint of low friction contact by implementing an efficient iterative algorithm, thus the algorithm can provide good accuracy even at high friction forces. It should

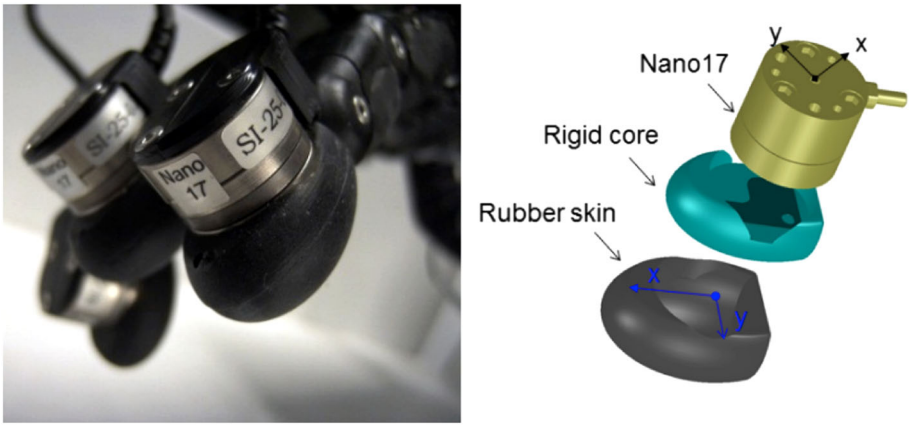

Fig. 1 The design of the fingertip with 2 mm rubber skin (outer layer)

be noted that, the output of the proposed method is a single contact location. Thus the use of the method is limited to the condition where the finger contacts the object at a single region in which the pressures are elliptically distributed. A contact sensing fingertip has been developed for this study. This finger is equipped with a 6-axis force/torque sensor and covered with a deformable rubber skin. The contact sensing fingertip was attached to the five digits of a Shadow^{TM} robotic hand and has been used to conduct surface following task for object exploration to demonstrate the advantages gained from the finger contact sensing algorithm.[1] The test results demonstrate the usefulness of the identified contact information from the contact sensing algorithm. The paper structure is organized as follows: (1) the introduction of the design of the fingertip and its instrumentation on the robotic hand; (2) the introduction of the contact sensing algorithm for a surface deformable fingertip; (3) the experimental evaluation of the contact sensing algorithm; (4) the application of the developed contact sensing fingertip for surface contour following.

2 The design of the fingertip and mechanical analysis of the rubber skin

2.1 Design of the fingertip

To implement the developed algorithm for contact sensing, an instrumented fingertip was designed. As shown in Fig. 1, the fingertip consists of a deformable rubber skin, a rigid core which is made of aluminium and a 6-DoFs ATI nano17 force/torque sensor (Calibration SI-25-0.25, resolution: 1/160 N for F_x, F_y, F_z, 1/32 Nmm for M_x, M_y, M_z, range: $F_x F_y = 25\,N$, $F_z = 35\,N$, M_x, M_y, $M_z = 250$ Nmm). The fingertip core is attached to the sensor and an outer layer of rubber.

To reduce the computational burden in the contact sensing algorithm, an ellipsoid shape for the outer rubber skin (covering the core) was chosen. The three semi-principal axes (a, b, c) of the ellipsoid skin have the lengths ($a = 9.5\,mm$, $b = 17\,mm$, $c = 10.5\,mm$). Poly 74-30 liquid rubber from Polytek^{TM} was used to construct the polyurethane rubber skin. The thickness of the rubber skin is 2 mm. The z axis of the Nano17 sensor is parallel to the z axis of the rubber skin. The x axis of the force sensor has a rotation angle of -120^o clockwise with respect to the x axis of the ellipsoid. The coordinate of the origin of the sensor in the ellipsoid frame is $[-\sin\alpha\ \cos\alpha\ 0]^T$, where $\alpha = 60^o$. The fingertip and sensor assembly attaches to the hand by means of modified distal phalange that is installed in place of the existing distal phalange to provide a mounting base that the sensor can be screwed onto, Fig. 2.

2.2 Mechanical analysis of the rubber skin

The use of a rubber skin on the fingertip brings the issue of surface deformation under compressive load. Therefore ini-

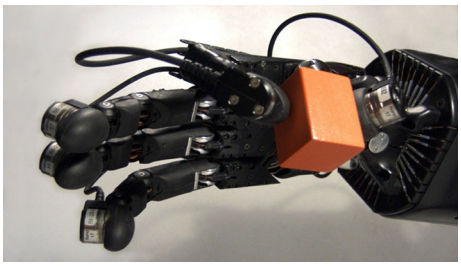

Fig. 2 The developed fingertips are attached to the five digits of the Shadow^{TM} hand

[1] The work presented in this paper has been done in collaboration between King's College London (KCL), Université Pierre et Marie Curie (UPMC) and Shadow Robot Company (Shadow) within the HANDLE project (grant agreement ICT 231640). KCL has contributed on the fingertip contact sensing algorithm, Shadow has contributed in the fingertip design and fabrication and UPMC has contributed on the finger force feedback control and the object surface exploration using the contact information identified by the fingertip. The object pose estimation using the finger has been done by KCL with contribution from UPMC.

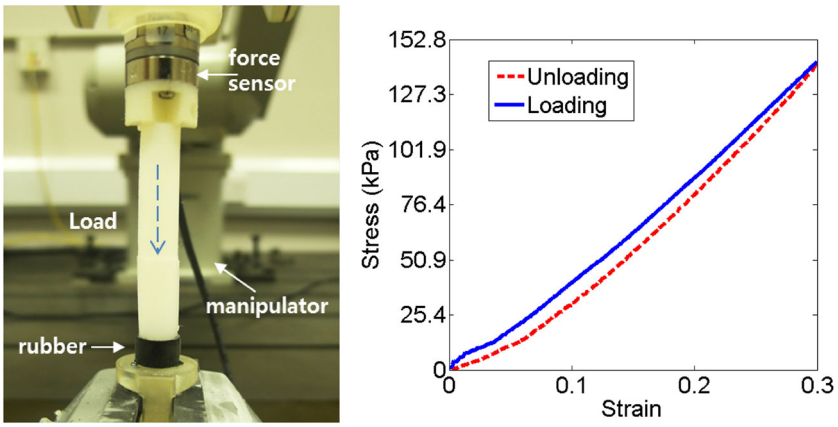

Fig. 3 The mechanical property test of the rubber material

tial tests were carried out to investigate the rubber mechanical properties. During these tests, a compressive load was applied to a cylindrical rubber sample (10 mm in diameter and 10 mm in height) using a RV-6SL Mitsubishi manipulator. The load was measured using an ATI Nano17 force/torque sensor, Fig. 3. During a test, the manipulator gradually compressed the rubber sample until 30 % strain was reached. This test was repeated three times; the averaged loading and unloading strain–stress curves are shown in Fig. 3. It can be seen that the rubber material has an almost linear strain–stress curve and very low hysteresis. The estimated Young's modulus of the rubber material is $E = 474.1$ kPa. Measured with different methods, the reported young's modulus of human skin fresh in literature ranges from around 800 to 25 kPa (Agache et al. 1980; Liang and Boppart 2010). Hence the rubber material is comparable to human skin tissue. Since the rubber skin has only 2 mm thickness and is covered on a rigid ellipsoid core, the relationship between the applied force F and the normal surface compression depth, Δd is expected to be highly nonlinear. To investigate such relationship, taking into account for the radius effects, various normal loads were applied to two different locations with the maximum and minimum local radius on the finger, A and B as shown in Fig. 4.

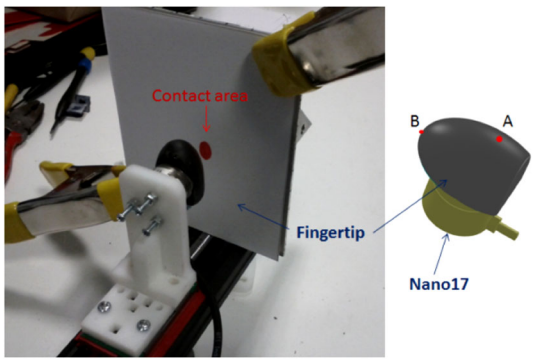

Fig. 4 Tests for investigating the relationship between the surface deformation and the external load. The *A* and *B* indicate the two testing locations on the fingertip

During each test, the fingertip was dyed with red colour and pushed towards a blank white paper glued on a rigid plate, applying different normal loads. The red dye of the contact area was translated from the finger to the white paper through the contact. Thus the contact area can be obtained by measuring the size of red print mark on the white paper, Fig. 4. The deformation Δd was then computed geometrically based on the size of contact area. Figure 5 shows the results from two locations A and B. It can be observed that there are two different force–displacement curves at location A and B. This is due to the difference in geometry of these two locations. The fingertip is an ellipsoid and the curvature at location A is larger than location B. Hence, under the same displacement along surface normal direction, there is more rubber material being compressed at location A than the being compressed at location B, Fig. 5. Thus, the larger the radius, the faster the normal load grows with the same increment of the Δd. However it can also been found that when the normal load is below 6 N, the two measurements are closed to each other. Since A and B have the maximum and minimum curvature on the ellipsoid surface, it is reasonable to assume that measurements at other locations will be within the boundary defined by the curves of A and B. We conclude that a single equation can be used to describe the deformation and normal load function for the whole area of the skin as long as the normal load is smaller than 6 N. Curve fitting by using measurements from both location A and B when normal load <6 N and rejecting high external loads data, as shown in Fig. 6, indicates that the function can be estimated as a linear or a quadratic function as:

$$\|\boldsymbol{F}_n\| = E(\Delta d) = \begin{cases} E_1 \Delta d \\ E_2 \Delta d^2 \end{cases}, \tag{1}$$

where $\|\boldsymbol{F}_n\|$ is the magnitude of the normal load, E_1 and E_2 are the elastic coefficients ($E_1 = 16.5$ N/mm, $E_2 = 43.38$ N/mm^2).

Although the rubber material has similar elasticity to human finger soft tissue, human finger pad has much thicker

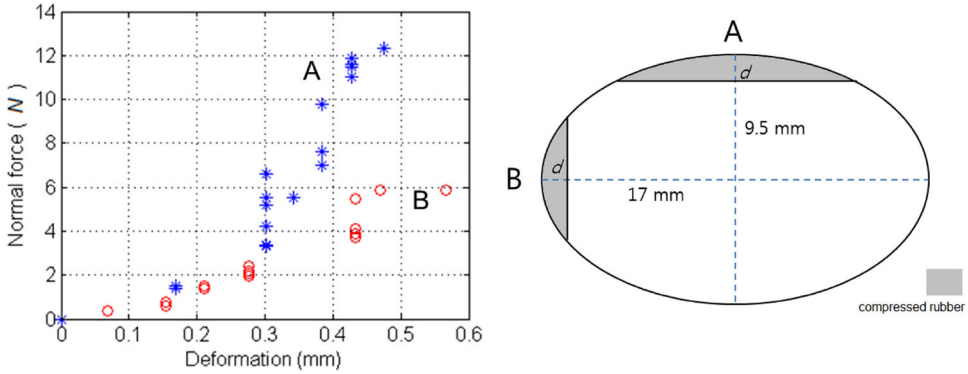

Fig. 5 The deformation versus the normal force for locations *A* and *B*, data points *asterisk* indicate results from location *A*, while *open circle* indicate results from location *B*. The *side view* of fingertip is shown on the *right*; the local curvature difference at *A* and *B* causes more rubber material being compressed at *A* than at *B* with the same normal compression distance *d*

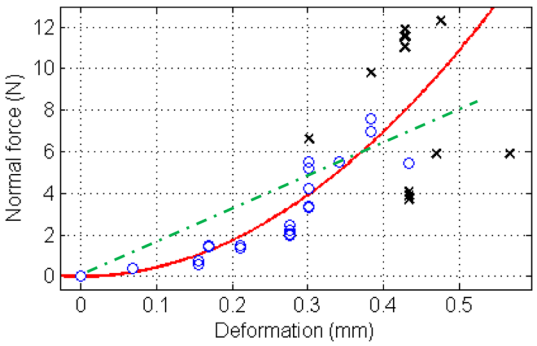

Fig. 6 The estimated function for the deformation Δd with respect to the normal force; the data points *open circle* show the selected measurements from both locations A and B used for function fitting, *times symbol* indicate the measurements rejected for fitting due to their high normal load or deformation. The *dashed line* indicates the linear function $F_n = E_1 \Delta d$ where $E_1 = 16.5\,\text{N/mm}$. The *solid line* shows the estimated quadratic function $F_n = E_2 \Delta d^2$, where $E_2 = 43.38\,\text{N/mm}^2$

soft tissue than the 2 mm rubber layer used in the developed finger. Thus the force–deformation depth ratio of the developed finger is about 16 times higher than the ratio of human finger pad reported in (Pawluk and Howe 1999). An increased softness in a robot finger would be desirable mechanically but would be more likely prone to high sensing errors.

3 The sensing algorithm

3.1 Modelling of the finger contact

Considering a general case and assuming no external load is applied, the fingertip is an ellipsoidal surface S_0 with radii a, b and c. Point **o** is the center of the ellipsoid as shown in Fig. 7. Our fingertip has the following parameters: $a = 9.5\,\text{mm}$, $b = 17\,\text{mm}$, $c = 10.5\,\text{mm}$. Assuming an object is in contact with the fingertip at a single location, the normal load causes the rubber skin deforming by Δd along the normal direction of the contact. Similar to the concept introduced in (Inoue and Hirai 2006), the rubber skin is assumed to consist of infinite virtual springs which can be compressed along the normal direction of surface. Since the rubber skin is glued onto a rigid core and is relative thin, its shear stiffness is high. Thus the lateral shear deformation introduced by the tangential load is small and is neglected in this study. The contact region of the object is assumed to be locally flat. Let the coordinates of the contact point to be $\boldsymbol{p_o} = [\mathrm{x}_0,\ \mathrm{y}_0,\ \mathrm{z}_0]^{\mathrm{T}}$ in the **o** frame, $\boldsymbol{p_o}$ can be considered to be laid on a virtual ellipsoid surface S where each of its axis is reduced by Δd with respect to S_0. Therefore, the coordinates of the contact location satisfy Eq. 2:

$$S\,(x_0, y_0, z_0) : \frac{x_0^2}{(a-\Delta d)^2} + \frac{y_0^2}{(b-\Delta d)^2} + \frac{z_0^2}{(c-\Delta d)^2} = 1 \tag{2}$$

Let **c** to be the origin of the force/torque sensor, and the coordinate of the contact location in frame **c** is $\boldsymbol{p_c} = [x,\ y,\ z]^T$. The coordinate of the origin of the sensor in the ellipsoid frame is represented as $[d_x\ d_y\ d_z]^{\mathrm{T}}$. The homogenous transformation between $\boldsymbol{p}_o$ and $\boldsymbol{p}_c$ is:

$$\begin{bmatrix} \boldsymbol{p}_o \\ 1 \end{bmatrix} = \begin{bmatrix} \boldsymbol{R_{oc}}^{\mathrm{T}} & -\boldsymbol{R_{oc}}^{\mathrm{T}}\,\vec{OC} \\ 0 & 1 \end{bmatrix} \begin{bmatrix} \boldsymbol{p}_c \\ 1 \end{bmatrix} \tag{3}$$

where $\vec{OC}$ represents $[d_x d_y d_z]^{\mathrm{T}}$ in the sensor's frame which is equal to $[-\sin(60^{\mathrm{o}})\ \cos(60^{\mathrm{o}})\ 0]^{\mathrm{T}}$, $\boldsymbol{R_{oc}}$ is the rotation transformation matrix,

$$\boldsymbol{R_{oc}} = \begin{bmatrix} \cos\theta & -\sin\theta & 1 \\ \sin\theta & \cos\theta & 0 \\ 0 & 0 & 0 \end{bmatrix},$$

where the angle θ is the angle of the x axis of the force sensor with respect to the x axis of the ellipsoid. In our design the rotation angle θ is -120^{o}. Applying the Eq. 3, the relationship between $\boldsymbol{p}_o$ and $\boldsymbol{p}_c$ is:

$$\begin{cases} x_0(x, y, z) = \cos\theta x + \sin\theta y - \cos\theta d_x - \sin\theta d_y \\ y_0(x, y, z) = -\sin\theta x + \cos\theta y + \sin\theta d_x - \cos\theta d_y \\ z_0\,(x, y, z) = z - d_z \end{cases} \tag{4}$$

Substitute Eq. 4 into Eq. 2, the surface equation with respect to the sensor frame $S\,(x, y, z)$ can be obtained. As

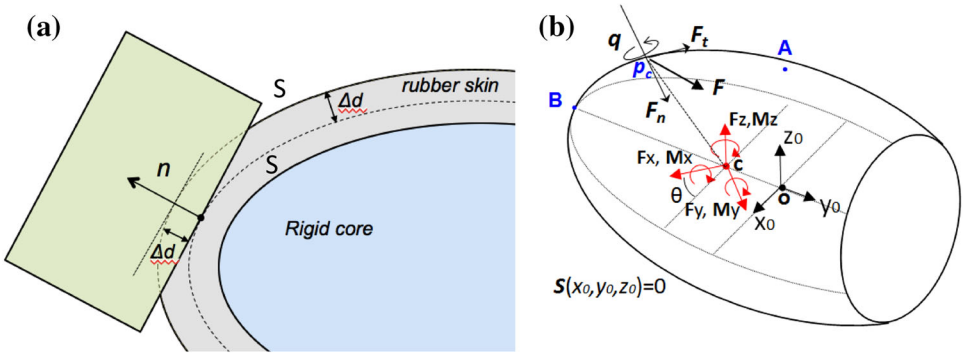

Fig. 7 The deformation of the rubber skin under normal force (**a**) and the force/torque-sensing diagram of the ellipsoidal fingertip (**b**)

shown in Fig. 7, the surface equation of the fingertip force is indicated using function $S(x, y, z)$, $\boldsymbol{F} = [f_x, f_y, f_z]^T$ and $\boldsymbol{M} = [\mathrm{m_x}\ \mathrm{m_y}\ \mathrm{m_z}]^{\mathrm{T}}$ are the measurements acquired using the force/torque sensor. It can be assumed that the local torque $\boldsymbol{q}$ is always perpendicular to the surface (Bicchi et al. 1993). Hence local torque $\boldsymbol{q}$ at a contact location $\boldsymbol{p_c} = [x,\ y,\ z]^{\mathrm{T}}$ can be described as $k\nabla S(\boldsymbol{p_c})$. Since the fingertip has mass and inertial, its own acceleration could affect the force/torque measurements, as well as the contact forces. When an external force $\boldsymbol{f}$ and local torque $\boldsymbol{q}$ interact with the finger while it is moving with a translational acceleration $\ddot{\boldsymbol{x}}$ and an angular acceleration $\ddot{\boldsymbol{\omega}}$, the following equilibrium equations hold:

$$\begin{cases} \boldsymbol{F} - \boldsymbol{f} = m\ddot{\boldsymbol{x}} \\ \boldsymbol{M} - \boldsymbol{p_c} \times \boldsymbol{f} + k\nabla S\left(\boldsymbol{p_c}\right) = I_{inertia}\ddot{\boldsymbol{\omega}} \end{cases} \tag{5}$$

where m is the mass of the fingertip and the $I_{inertia}$ is the moment of inertia matrix. In this study, the finger's motion is assumed to be quasi-static, i.e. $\ddot{\boldsymbol{x}}, \ddot{\boldsymbol{\omega}}$ close to zero. Since the designed fingertip has a light mass and a low moment of inertia, the above equation can be simplified as:

$$\boldsymbol{p_c} \times \boldsymbol{F} + k\nabla S\left(\boldsymbol{p_c}\right) = \boldsymbol{M} \tag{6}$$

Defining $\boldsymbol{Q} = \nabla S(\boldsymbol{p}_c)$ as the normal vector of the contact location shown in Fig. 6 and given a contact location $\boldsymbol{p}_{\mathrm{c}} = [x,\ y,\ z]^{\mathrm{T}}$, the normal force $\boldsymbol{F_n}$ and tangential force $\boldsymbol{F_t}$ can be expressed as: $\boldsymbol{F_n} = \boldsymbol{Q}\frac{\boldsymbol{Q}^T\boldsymbol{F}}{\boldsymbol{Q}^T\boldsymbol{Q}}$ and $\boldsymbol{F_t} = \boldsymbol{F} - \boldsymbol{F_n}$

where $\boldsymbol{Q} = \left[\frac{\partial S}{\partial x}, \frac{\partial S}{\partial y}, \frac{\partial S}{\partial z}\right]^{\mathrm{T}}$ *and*

$$\begin{cases} \frac{\partial S}{\partial x} = 2\left(\frac{\cos\theta x_0(x,y,z)}{(a-\Delta d)^2} - \frac{\sin\theta y_0(x,y,z)}{(b-\Delta d)^2}\right) \\ \frac{\partial S}{\partial x} = 2\left(\frac{\sin\theta x_0(x,y,z)}{(a-\Delta d)^2} + \frac{\cos\theta y_0(x,y,z)}{(b-\Delta d)^2}\right) \\ \frac{\partial S}{\partial x} = \frac{2z_0(x,y,z)}{(c-\Delta d)^2} \end{cases} \tag{7}$$

As demonstrated in the Sect. 2.2, the rubber skin deformation along the normal direction of the contact, Δd, satisfies the Eq. 1 Thus the following equation holds

$$\left\| \boldsymbol{Q}\frac{\boldsymbol{Q}^T\boldsymbol{F}}{\boldsymbol{Q}^T\boldsymbol{Q}} \right\| = \|\boldsymbol{F_n}\| = E(\Delta d) \tag{8}$$

Based on the above analysis it can be seen that under a single location contact between the finger and an object, the contact location, the rubber skin deformation and the force/torque measurement should satisfy the following set of equations.

$$\begin{cases} \boldsymbol{p_c} \times \boldsymbol{F} + k\nabla \boldsymbol{S}(\boldsymbol{p_c}) = \boldsymbol{M} \\ S\left(\boldsymbol{p}_0\right) = 0 \\ \|\boldsymbol{F_n}\| = E(\Delta d) \end{cases} \tag{9}$$

It can be seen from above that the contact location, the local torque and the skin deformation can be described using a vector $\mathbf{x} = [x\ y\ z\ k\ \Delta\ d]^{\mathrm{T}} = [\boldsymbol{p}_c\ k\ \Delta d]^{\mathrm{T}}$. Thus the problem of identifying $\mathbf{x}$ is equivalent to solving $\boldsymbol{g}(\mathbf{x}) = 0$:

$$\boldsymbol{g}\left(\mathbf{x}\right) = \begin{bmatrix} k\frac{\partial S}{\partial x} - f_y z + f_z y - m_x \\ k\frac{\partial S}{\partial y} - f_z x + f_x z - m_y \\ k\frac{\partial S}{\partial z} - f_x y + f_y x - m_z \\ S(xyz) \\ \|\boldsymbol{F_n}\| - E(\Delta d) \end{bmatrix} = 0, \tag{10}$$

While $\boldsymbol{g}(\mathbf{x})$ is nonlinear, it has been proven in (Bicchi et al. 1993) that when the contact surface is convex there is a unique solution for the contact location identification with 6-DoFs force/torque measurements. Since the rubber skin has a convex ellipsoid shape, thus the contact information $\mathbf{x}$ can be obtained by identifying the roots of $\boldsymbol{g}(\mathbf{x}) = 0$ without further analysis.

3.2 Iterative method for solving $g(x)$

Levenberg–Marquardt (LM) is a gradient-based iterative method for nonlinear parameter estimation. It has been shown that the LM algorithm has superior performance compared with other gradient-based methods for nonlinear parameter estimation, achieving a fast convergence time and good robustness with regards to the algorithm initial guess (Bard 1970). Therefore, we use the LM algorithm to solve $\boldsymbol{g}(\mathbf{x}) = 0$. First a positive definite function χ^2 is defined to guarantee the solution is the global minimum of the function as the follows.

$$\chi^2 = \frac{1}{2}\mathbf{g}(\mathbf{x})^T\mathbf{g}(\mathbf{x}) \tag{11}$$

Estimating the parameter vector $\mathbf{x} = [x\ y\ z\ k\ \Delta d]^{\mathrm{T}}$ is thus the problem of minimizing χ^2. The derivative of the function χ^2 with respect to estimated parameters is:

$$\frac{\partial \chi^2}{\partial \mathbf{x}} = \mathbf{g}(\mathbf{x})^T \frac{\partial \mathbf{g}(\mathbf{x})}{\partial \mathbf{x}} = \mathbf{g}\,(\mathbf{x})^T\,\mathbf{J}(\mathbf{x})$$

where $\mathbf{J}(\mathbf{x})$ is the Jacobian matrix of $\boldsymbol{g}(\mathbf{x}), \mathbf{J}\,(\mathbf{x}) = \frac{\partial g(\boldsymbol{X})}{\partial \boldsymbol{X}}$. Applying the LM method, the parameter vector $\mathbf{x}$ can be iteratively estimated using the following rule:

$$\begin{aligned} \mathbf{h} &= -\left[\mathbf{J}^T\mathbf{J} + \lambda \mathrm{diag}\left(\mathbf{J}^T\mathbf{J}\right)\right]^{-1}\mathbf{J}^T\mathbf{g}(\mathbf{x}) \\ \mathbf{x}_{k+1} &= \mathbf{x}_k + \mathbf{h}, \end{aligned} \tag{12}$$

where $\mathbf{h}$ is the perturbed step. A large value of parameter λ leads to a gradient descent update while small value of parameter λ leads to a Gauss-Newton update. When the current estimate is far from its real value, then the $\mathbf{h}$ is updated using a large λ; when the current estimate becomes close to its real value, then the value of λ is adaptively reduced. The condition of adaptively changing λ is computed as Eq. 13 (Madsen et al. 2004)

$$\chi(\mathbf{x}_k)^2 - \chi(\mathbf{x}_{k+1})^2 > \varepsilon_1 \mathbf{h}^T\left[\lambda\mathbf{h} - \mathbf{J}^T\mathbf{g}(\mathbf{x})\right] \tag{13}$$

If the condition holds, then λ is reduced by a factor of ten; otherwise, λ is increased by a factor of ten. Parameter ε_1 is a small positive number and was set to 10^{-2}. Since a good initial guess could significantly improve the convergence speed of an iterative method, the algorithm first decides the initial guess of the contact location based on the direction of the resultant force vector $\mathbf{F}$. Based on the diagram of Fig. 7, and defining $\mathbf{O} = [\mathbf{y}_0,\ \mathbf{z}_0]$, $\mathbf{O}$ is 3×2 matrix, the projection vector of $\mathbf{F}$ to the y_0z_0 plane is $[p_1\,p_2\,p_3]^{\mathrm{T}} = \mathbf{O}\left(\mathbf{O}^{\mathrm{T}}\mathbf{O}\right)^{-1}\mathbf{O}^{\mathrm{T}}\mathbf{F}$. If $p_2 \geq 0$, i.e. $\mathbf{F}$ points towards the positive $\mathbf{y}_0+$ axis of the ellipsoid, or $p_3 \geq 0$, i.e. $\mathbf{F}$ points to $\mathbf{z}_0^+$ axis, the initial contact location is assumed at location B. Otherwise, the initial contact location is assumed at location A. Then the g(x) = 0 is solved iteratively to estimate the contact location, the magnitude of local torque and the normal surface deformation. After the iterative algorithm converge, the surface normal, normal force vector, tangential force vector and local torque vector are computed and provided to the hand controller. The developed algorithm for the fingertip contact sensing is illustrated in the following pseudo code.

Algorithm 1 Intrinsic Contact Sensing

Input: $[f_x, f_y, f_z, m_x, m_y, m_z]$ ▷ read(force sensor)
$\mathbf{F} = [f_x, f_y, f_z]^T$
if $F^T z_0 > 0 \vee F^T y_0 > 0.5\|F\|$ **then**
  $\mathbf{p}_{initial} = location\,\boldsymbol{B}$: $[-sin\alpha - bsin\theta, cos\alpha + bcos\theta, 0]$
  $\mathbf{x}_{initial} = [\mathbf{p}_{\mathbf{initial}}, 00]$
else
  $\mathbf{p}_{initial} = location\,\boldsymbol{A}$: $[-sin\alpha, cos\alpha, c]$
  $\mathbf{x}_{initial} = [\mathbf{p}_{\mathbf{initial}}, 0, 0]$
end if
$[\mathbf{p}_c, k\Delta d] \leftarrow$ Solve $\mathbf{g}(\mathbf{x}) = 0$ ▷ Iterative optimization
▷ $\mathbf{p}_c$: coordinates of contact location in sensor frame
$\hat{n} = \nabla S(\mathbf{p}_c)$ ▷ Find normal direction
Normal Force: $\mathbf{F}_n \leftarrow$ Projection of $\mathbf{F}$ into $\hat{n}$
Tangential Force: $\mathbf{F}_t \leftarrow \mathbf{F} - \mathbf{F}_n$
Local Torque: $\mathbf{q} \leftarrow k\nabla S(\mathbf{p}_c$
Output: : $[\mathbf{p}_c, \mathbf{q}, \mathbf{F}_n, \mathbf{F}_t, \Delta d]$

It was experimentally observed that the iterative algorithm had very good convergence with the use of the linear function of Eq. 1. With the quadratic function of Eq. 1, the algorithm tended to diverge and was sensitive to the initial guess. This may be due to the use of a quadratic term creating additional local minima where the gradient descent search of LM could get trapped. The theoretical analysis of the algorithm convergence with the quadratic function or the higher order elasticity function of the rubber material is beyond the scope of this paper. Hence the linear function of Eq. 1 was selected for the contact sensing algorithm in this study.

4 Contact sensing evaluation

4.1 Contact location estimation

Validation tests have been carried out in order to validate the accuracy of the contact sensing algorithm. For validating the accuracy of the contact location identification, a test rig was setup as shown in Fig. 8. 13 location markers were painted in white on the fingertip surface, Fig. 9. The coordinates of the markers were measured using a robot manipulator (Mitsubishi RV-6SL) with the position accuracy of 0.01 mm. Since local area contact with a finger occurs mostly during object grasping, a probing device which consisted of transparent Perspex glass with a red central mark and endoscope camera was developed and used to contact all the individual white markers. The Perspex glass provides a local area contact with the finger and allows the centroid of the contact to be visually inspected.

During a contact, the probing device was adjusted to be perpendicular to the finger surface and to coincide the red mark on the Perspex with the centroid of one white marker. The contact force was monitored to be in the range of 1–6 N. This procedure was repeated four times and the estimated contact locations were compared with the ground-truth values.

The estimation results of contact locations are illustrated in Fig. 9b, c. It can be seen that the contact locations were

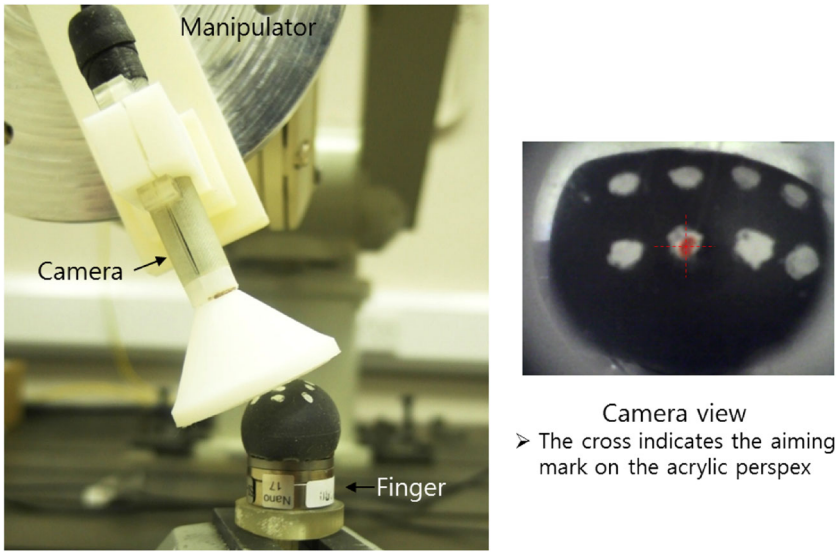

Fig. 8 The test set-up for evaluating the contact location estimation; a probing device consisting of a Perspex glass and an endoscope camera was used to touch 13 marked locations on the fingertip

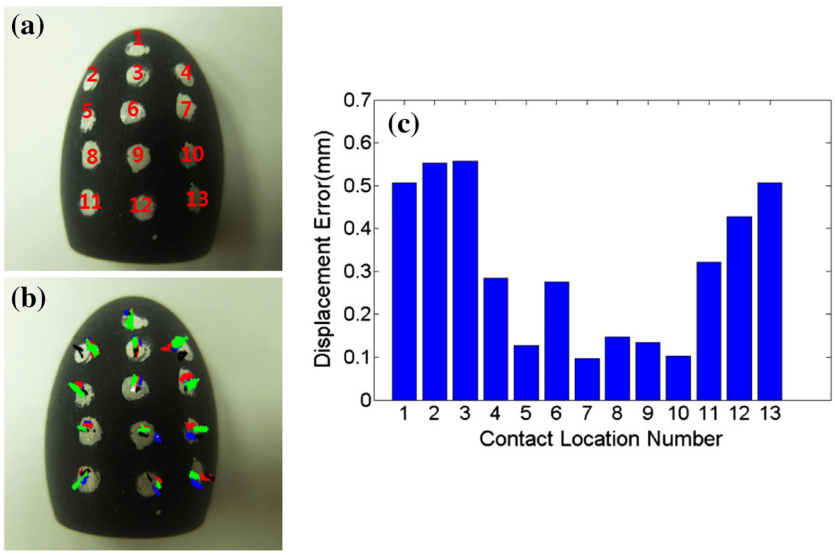

Fig. 9 The locations of the 13 markers are shown in (**a**); results of contact location estimation for the 13 location are shown in (**b**); the *red*, *green*, *blue* and *black markers* indicate the estimated contact locations from four different tests; **c** shows the estimation error, the maximum location error is below 0.55 mm (Color figure online)

accurately identified for all the 13 locations; the average root mean square error (RMSE) is 0.33 mm, with the maximum error <0.55 mm. It was observed that: although the contact sensing algorithm assumes a single point contact, the algorithm can cope with single area contact very well in practice. It can be seen from the experimental results that when the finger is in contact with an area, the algorithm identifies the centroid of the contact area as the contact location. It is also seen from Fig. 9c that errors of contact location estimation at the peripheral locations 1, 2, 3, 4, 11, 12, 13 are considerably higher than those at central locations 5–10. This phenomenon may be due to the measurement errors of the force/torque sensor. Since contact forces at peripheral locations generate higher moments than those at central locations, the measurement errors tend to be magnified through the moment calculation in Eq. 9, leading to increased errors when estimating the contact location $\boldsymbol{p}_c$.

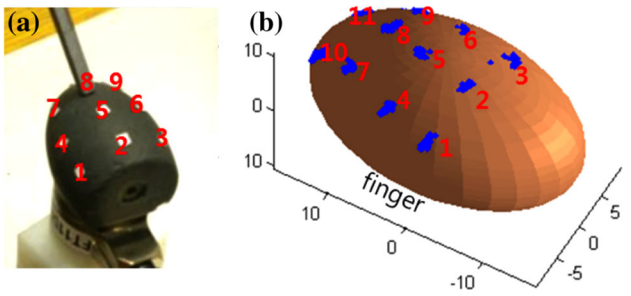

Fig. 10 **a** The test setup for evaluating the accuracy of contact location estimation for small radius contacts, **b** estimation results (the *blue dots*) overlaid on the finger surface model (Color figure online)

For evaluating the accuracy of the contact location estimation when the object has small radius, 11 locations were marked on the fingertip and measured using the robot manipulator following the same procedure shown above, Fig. 10a.

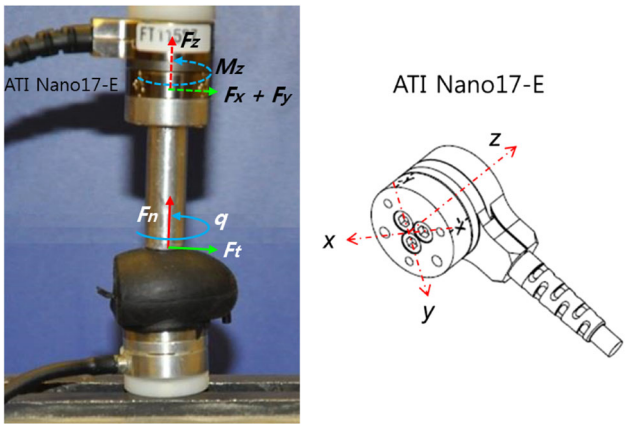

Fig. 11 The test set-up for validating the estimation accuracy of the contact sensing finger in terms of the normal force, $\boldsymbol{f_n}$, the friction force, $\boldsymbol{f_t}$, and the local torque, $\boldsymbol{q}$; an ATI nano17-E force/torque sensor was used for bench marking; the sensor's z axis is aligned with the vector $\boldsymbol{f_n}$ and $\boldsymbol{q}$, the x–y plane is parallel with the tangential plane of the contact location

During tests, a thin rod tip was used to touch each marked location 10 times. The contact forces were between 0.5 and 3 N. The identified contact locations were compared with the ground-truth values. The results show that the RMSE of the estimated contact location is 0.32 mm which is comparable to the accuracy of the flat area contact shown in Fig. 9.

4.2 Contact forces estimation

To validate the estimation accuracy of the estimation error for normal force, friction force and the local torque, a test rig was set up as shown in Fig. 10. A six-axial ATI Nano17-E force/torque sensor was used as the benchmark sensor. The used benchmark sensor has a flat end-surface which is perpendicular to its z axis. When the benchmark sensor is in contact with the fingertip surface, the z axis of the benchmark sensor is coincident with the surface normal direction, Fig. 11. Thus the torque measured around the z axis of the benchmark sensor, m_z, is the local torque generated at the finger surface; the force measured along the z axis of the benchmark sensor, the f_z, equals to the normal force f_n; the magnitude of the resultant force of f_x and f_y of the benchmark sensor equals to the friction force, f_t.

To evaluate the sensing accuracy with respect to the applied magnitudes of friction force and local torque, experiments were conducted under three different conditions. (1) low local torque condition (Fig. 12): f_n (0–8.5) N, f_t (0–4) N, $q < 0.9$ Nmm, (2) low friction force condition (Fig. 13): f_n (0–6) N, q (−10 to 10) Nmm, $f_t < 0.4$ N; (3) high friction and local torque condition (Fig. 14): f_n (0–10) N, f_t (0–3) N, q (−10 to 0) Nmm. During these evaluation tests, the benchmark device was guided by hand to bring the fingertip into contact with the central top location of the fingertip to apply forces and torque as indicated in Fig. 11. The estimation accuracy is summarized in Table 1. Several observations can be made from Figs. 12, 13, and 14 and Table 1. First, high friction force f_t appears to be the main reason for a high estimation error. The estimation errors for f_n, f_t and q are all increased with the increase of f_t. It can be seen from Figs. 12 and 14 that when $f_t < 2.5$ N, both estimated f_n and f_t match very well with the benchmark values, while when $f_t > 2.5$ N, the deviations between the estimations and benchmarks become notable. Second, when f_t is low, the increase of local torque has limited effect on the estimation accuracy. It can be seen in Fig. 13 that the estimation errors of f_n and q are small despite the considerably large local torque being applied. In addition, the combination of high friction force and local torque will increase estimation error considerably. As shown in Fig. 14 and Table 1, the estimation errors increase 2–3 times when both high friction and local torque are applied compared to condition 1 and 2 (as shown in Figs. 12 and 13 respectively), indicating a limitation of the proposed contact sensing algorithm. However, it can be seen that the estimation error under the worst-case is still relatively low (4.5 % for f_n, 18.9 % for f_t and 27.8 % for q). Hence the proposed algorithm represents a promising approach to estimate the instantaneous f_n, f_t and q in robotic applications.

4.3 Limitation tests

Additional tests have been carried out to identify the practical limitations of the proposed method for contact sensing with respect to the apply forces and the local torque. All tests were conducted at a single location which was chosen at the centre top location A ($x = 0$, $y = 0$) on the fingertip, as shown in Fig. 7b. To evaluate the limitation associated with the friction force, the benchmark sensor shown in Fig. 11 was manually held to contact the fingertip vertically at location A and horizontally apply friction forces along the y-axis. To obtain high friction force levels, a rubber tape (friction coefficient (FC) ≈ 1.0) and a double-sided tape (FC ≈ 2.3) was glued on the flat end of the benchmark sensor respectively. Friction tests were repeated three times for both the double-sided tape and the rubber tape.

Contact sensing results are shown in Fig 15. It can be seen that, with FC ≈ 1.0, the estimation error of the contact location is still acceptable and the estimated contact locations are coincident with the experimental observation. However, with FC ≈ 2.2, the errors of the contact location estimation become significant and diverged from the location A. The errors that occur for high friction forces probably result from internal strains and stresses in the distorted rubber that shift the pressure distribution to a non-elliptical pattern which cannot be coped with by the proposed method. To evaluate the limitation of the algorithm associated with the applied local

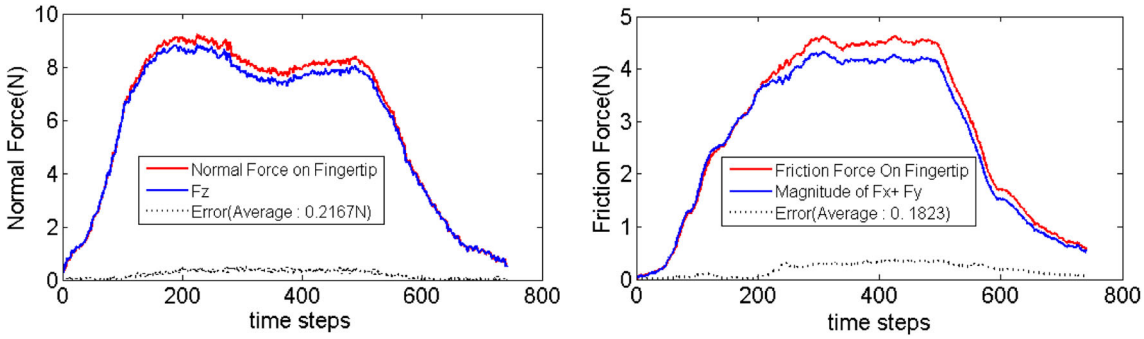

Fig. 12 The estimation of the normal force, f_n (*left*) and the friction force, f_t (*right*) when applying a low local torque q(<0.9 Nmm) as well as the estimation errors; the *blue solid lines* are the benchmark values, the *red solid lines* are the estimation results; the *black dotted lines* are the estimation errors (Color figure online)

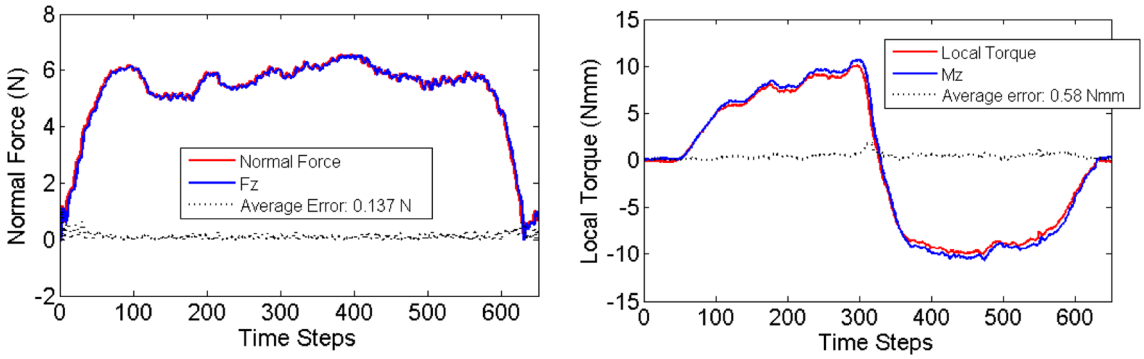

Fig. 13 The estimation of the normal force, f_n (*left*) and local torque q (*right*) when applying a low friction force, f_t, (<0.4 N) as well as the estimation errors; the *blue solid lines* are the benchmark values, the *red solid lines* are the estimation results; the *black dotted lines* are the estimation errors (Color figure online)

torque, similar procedures as the local torque evaluation tests described in Sect. 4.2 were conducted at the location A. Due to the limitation of the force/moment range of the Nano17 force sensor, local torque with the maximum magnitude of 16 Nmm was applied. It can be seen that the algorithm provides accurate estimation within the tested range of local torque, indicating a good robustness against the high local torque, Fig. 16. The algorithm limitation associated with the compressive normal force was also investigated. During the test, the normal force was applied at location A and was incrementally increased and decreased using a linear guide. The results show that the algorithm is very robust against the normal compressive force, Fig. 16.

The computation costs of the algorithm is evaluated using Matlab™ on a PC (2.40GHz Intel® CoreTM 2 Duo processor and 2GB RAM). It was found that the algorithm takes 7–42 iterations to converge. The average computation time for the contact sensing is between 158 and 242 Hz. Experimental evaluations show that the proposed iterative algorithm has very robust performance. The robustness may come from: (1) the uniqueness of the solution for the convex shape contact as proven in (Bicchi et al. 1993), resulting in a single global minimum for the cost function g(x) used in the iterative method; (2) the existence of a single global minimum in g(x) helps the algorithm to find an approximated solution in a gradient descent manner even when noise and measurement error exist. The developed algorithm has been implemented under Robot Operating System (ROS) platform, providing the outputs at 100 Hz (10 ms) to the hand controller which is described in the following section. Under ROS, force/torque sensor sampling rate is set at 1,000 Hz (1 ms), the computation time of the contact sensing algorithm for each given force/torque measurements is 4–6 ms. Hence the algorithm computation speed is suitable for the overall control loop.

5 Surface following for object exploration

5.1 Contour following algorithm

Surface exploration by touch could provide rich information such as surface local geometry, texture and friction properties (Okamura and Cutkosky 2001; Liu et al. 2012a). In this paper, we develop a control algorithm to use the developed contact sensing finger to follow the surface of an unknown object for obtaining the surface characteristics including surface geometry and friction coefficient. Given an unknown or partially known rigid surface S, the objective of the

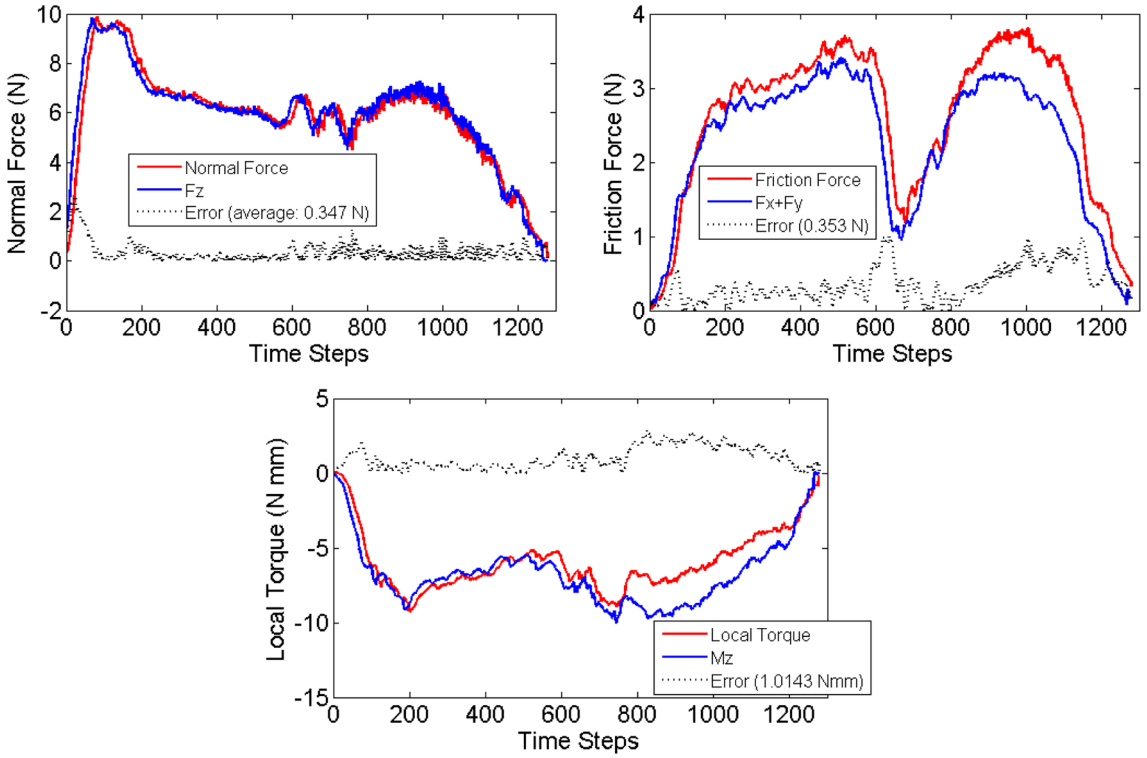

Fig. 14 The estimation of the normal force, $\boldsymbol{f_n}$ (*top left*), the friction force, $\boldsymbol{f_t}$,(*top right*) local torque $\boldsymbol{q}$ (*bottom*) as well as the estimation errors; the *blue solid lines* are the benchmark values, the *red solid lines* are the estimation results; the *black dotted lines* are the estimation errors (Color figure online)

Table 1 The mean and maximum errors of estimating the normal force, friction force and local torque

	Error f_n (N) mean (max)	*Error* f_t (N) mean (max)	*Error* q (Nmm) mean (max)
Condition-1: f_n 0–8.5 N, f_t 0–4 N, $\boldsymbol{q}$ 0–1.2 Nmm	0.217 (0.332)	0.182 (0.393)	0.563 (0.855)
Condition-2: f_n 0–6 N, f_t 0–0.4 N, $\boldsymbol{q}$ −10 to 10 Nmm	0.137 (0.182)	0.097 (0.237)	0.583 (0.783)
Condition-3: f_n 0–10 N, f_t 0–3 N, $\boldsymbol{q}$ −10 to 0 Nmm	0.347 (0.396)	0.353 (0.612)	1.014 (2.012)

algorithm is to move the fingertip from points A' (initial position) to B' (final position) while maintaining the contact to the surface S with a constant magnitude of normal force f_n where $f_n = \|\boldsymbol{F}_n\|$, Fig. 17. During this movement, the surface geometry and friction coefficient can be then estimated based on the estimation of contact position, contact force and contact normal in frame (O).

Obtaining the contact surface normal is essential for a contour following task, since the contact force control and instantaneous finger motion control rely on the directions of surface normal vector and its orthogonal counterpart, the tangential vector. Most of existing works described in the literature either assume that the end-effector is frictionless so that the resultant force is equal to the normal force (Jatta et al. 2006; Bossert et al. 1996) or use a vision system to capture the surface geometry (Chang 2004). The advantage of using our contact sensing algorithm together with the developed fingertip is that the surface normal of contact can be identified in real-time without the prior-knowledge of the surface geometry. This is especially useful in the context of dexterous hand manipulation where vision often has difficulties for surface estimation due to image occlusion by fingers.

Assuming that the robot palm position $\boldsymbol{X}_{palm}$ and orientation $\boldsymbol{R}_{palm}$ are known and $\Theta = [q_1, q_2, q_3, q_4]^T$ is the vector of joint position, the fingertip position $\mathbf{X}_f$ and orientation $\mathbf{R}_f$ can then be calculated with the help of the finger forward kinematic model.

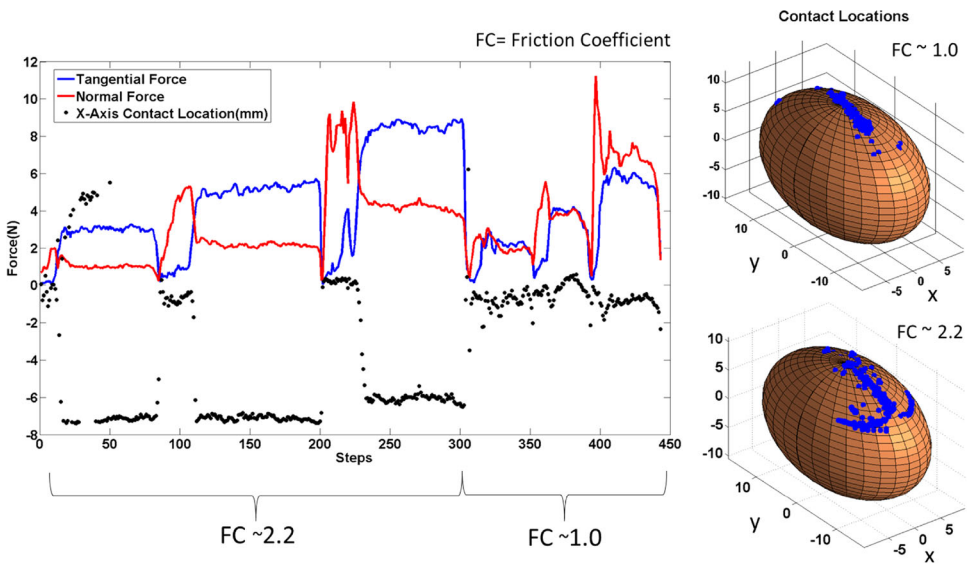

Fig. 15 The estimated contact locations under high friction coefficient (FC) contacts; the tangential and normal force are measured using the benchmark sensor. The results show that the algorithm provides accurate estimation when FC $\approx$ 1.0, however fails when FC is above 2 (Color figure online)

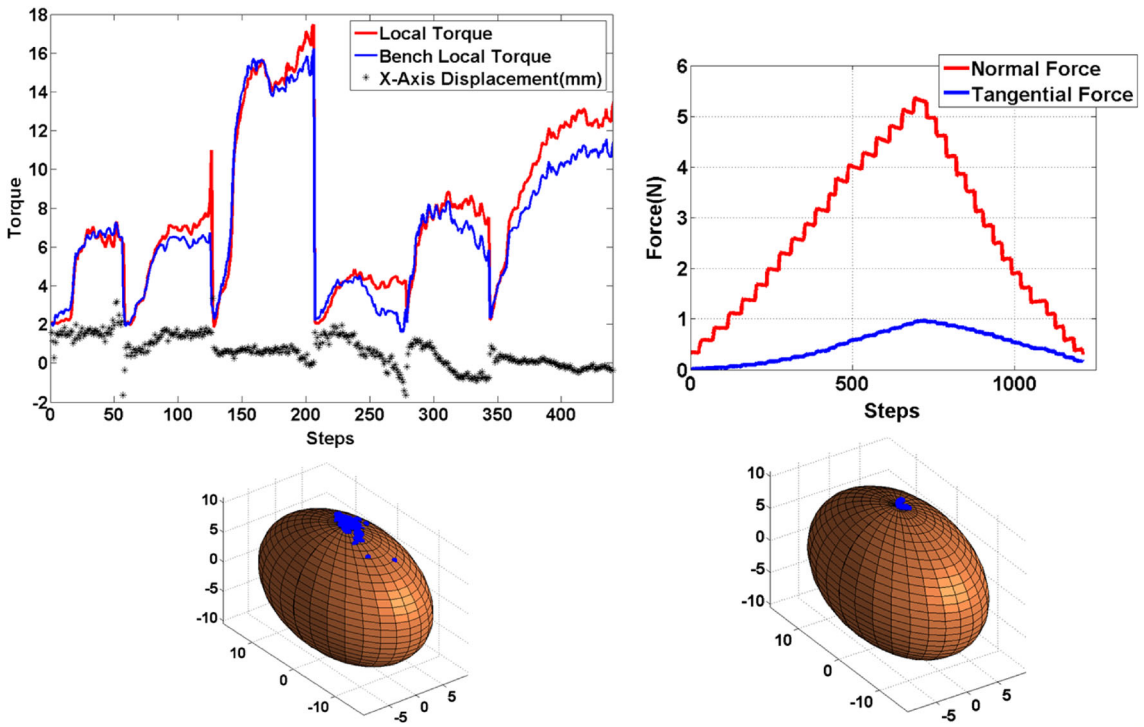

Fig. 16 The estimated contact locations under high local torque and compressive normal force. Bench local torques is measured using the benchmark sensor. The results show that the algorithm provides accurate estimation for normal compression and good accuracy with high local torque (Color figure online)

When the fingertip is in contact with S, the fingertip sensor gives the measures of the contact force $\boldsymbol{F}_{(\boldsymbol{T})}$, contact local torque $\boldsymbol{q}_{(\boldsymbol{T})}$, contact location $\boldsymbol{p}_{(\boldsymbol{T})}$ and contact normal $\boldsymbol{e}_{n(\boldsymbol{T})}$. The subscript $(\boldsymbol{T})$ means that the data is given in the fingertip frame $(\boldsymbol{T})$. The conversion of data from fingertip frame $(\boldsymbol{T})$ to robot base frame $(\boldsymbol{O})$ can be conducted as follows (the subscripts of data in frame $(\boldsymbol{O})$ are omitted):

$$\begin{aligned} \boldsymbol{F} &= \mathbf{R}_f \boldsymbol{F}_{(\boldsymbol{T})} \\ \boldsymbol{q} &= \mathbf{R}_f \boldsymbol{q}_{(\boldsymbol{T})} \\ \boldsymbol{e_n} &= \mathbf{R}_f \boldsymbol{e_{n(T)}} \\ \boldsymbol{p} &= \boldsymbol{X}_f + \mathbf{R}_f \boldsymbol{p}_{(\boldsymbol{T})} \end{aligned} \tag{14}$$

In order to exploit that control scheme, the fingertip is modelled as a virtual particle C with nominal mass m to

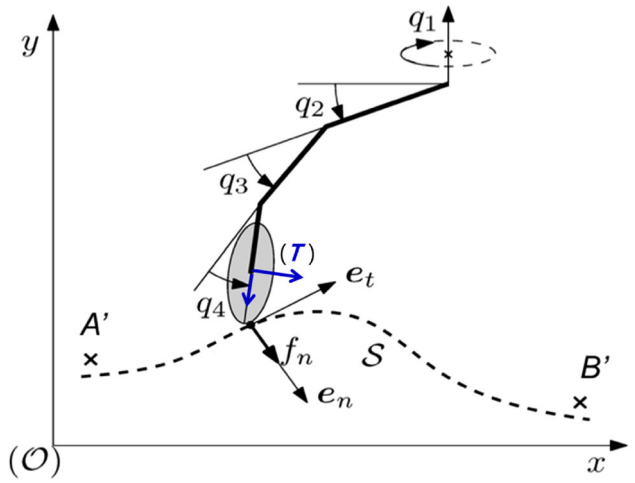

Fig. 17 Sketch of a fingertip following a contour where frame (O) refers to the robot base and (T) refers to fingertip frame (frame in which the sensor measurements are given)

simplify the algorithm. The contact location change in the finger frame due to its rolling motion with respect to the surface is not considered. There are three forces applied to this particle: the active fingertip force $\boldsymbol{F}_a$, the object surface reactive $\boldsymbol{F}_r$ and the gravitational force $m\boldsymbol{g}$ where $\boldsymbol{g}$ is the gravitational acceleration. The active contact force $\boldsymbol{F}_a$ can be decomposed into two components: the normal force $\boldsymbol{F}_{an}$ and the tangential force $\boldsymbol{F}_{at}$ as shown in Eq. 10. In order to make the finger move while in contact, $\boldsymbol{F}_{at} \geq k_{fr}\boldsymbol{F}_{an}$, where k_{fr} is the dry friction coefficient at the contact position. To effectively control the active contact force $\boldsymbol{F}_a$ exerted by the fingertip, a force controller combining the direct (torque-based) and the indirect (position-based) approaches by adjusting the joint torque saturation limit (max-torque) has been used. The details of this force controller are described in (Nguyen and Perdereau 2013). For simplicity, we only consider a control scheme for a dimensional case where the gravitational force of the finger can be balanced by the object surface. Thus, the gravitational force can be neglected to simplify the calculation. Consequently, the dynamics of this virtual particle is governed by the following equation:

$$m\boldsymbol{a} = \boldsymbol{F}_a + \boldsymbol{F}_r$$

where $\boldsymbol{a}$ is particle acceleration. Projecting this equation on $\boldsymbol{e}_n$ direction and tangential plan, the following equations are obtained (object surface is supposed to be fixed):

$$0 = m\boldsymbol{a}_n = \boldsymbol{F}_{an} + \boldsymbol{F}_{rn}$$
$$m\boldsymbol{a}_t = \boldsymbol{F}_{at} + \boldsymbol{F}_{rt}$$

In this study, static friction model of the contact is applied. Since the contact point velocity is small, the dry friction coefficient is used (Olsson et al. 1998). Consequently, the tangential reaction force can be approximated by: $\boldsymbol{F}_{rt} = k_{fr}\boldsymbol{F}_{rn}$. In this situation, the contact position can be entirely controlled by acting on $\boldsymbol{F}_{at}$ with a proportional-integral PI control to reduce the position error $(\boldsymbol{p}_d - \boldsymbol{p}_c)$, where $\boldsymbol{p}_d$ is the desired contact position and $\boldsymbol{p}_c$ is the current contact position. To smooth the contact velocity, an intermediate variable $\boldsymbol{p}_r$ is created as temporary desired position or reference position and the PI action is calculated over this variable, not on $\boldsymbol{p}_d$. Let T_s be the sampling time of the control loop ($T_s = 0.01$ s). $\boldsymbol{p}_r$ is generated by the following formula:

$$\boldsymbol{p}_r = \begin{cases} \boldsymbol{p}_i + V_d \frac{\boldsymbol{p}_d - \boldsymbol{p}_i}{\|\boldsymbol{p}_d - \boldsymbol{p}_i\|} T_s, & if\ T_s < \frac{\|\boldsymbol{p}_d - \boldsymbol{p}_i\|}{V_d} \\ \boldsymbol{p}_d, & if\ T_s \geq \frac{\|\boldsymbol{p}_d - \boldsymbol{p}_i\|}{V_d} \end{cases} \quad (15)$$

where $\boldsymbol{p}_i$ is the initial contact position and V_d is a pre-set velocity constant. Given a fixed velocity V_d and the time interval of each control step, Eq. 15 indicates that the finger will move to $\boldsymbol{P}_d$ if it is reachable given the time and velocity, otherwise it will move along the direction of the vector $\boldsymbol{p}_d - \boldsymbol{p}_i$ as far as possible. Once the reference position p_r is calculated, the desired tangential force $\boldsymbol{F}_{td}$ (or $\boldsymbol{F}_{at}$) is obtained through PI control as:

$$\boldsymbol{F}_{td} = K_p\left(\boldsymbol{p}_r - \boldsymbol{p}_c\right) + K_p \sum_0^i (\boldsymbol{p}_r - \boldsymbol{p}_c) T_s$$

where K_p and K_I are the proportional and integral gains. The normal desired force $\boldsymbol{F}_{nd}$ is determined by $\boldsymbol{F}_{nd} = f_{nd}\boldsymbol{e}_n$, where f_{nd} is the desired normal force and $\boldsymbol{e}_n$ is the current contact surface normal.

5.2 Experimental results of surface following

Experiments have been carried out using both simulations and a Shadow^{TM} robot hand. The simulation has been done using Anykode Robotics Simulator with ODE as physical engine. In the simulation, the robot hand has the same kinematic characteristics as the real one. It is also equipped with a sensor similar to the real one at the fingertip. In the simulation, the robot hand was demanded to move its fingertip from one position to another one on a curved surface that is unknown to the robot. During the movement, the robot is required to maintain the contact with the surface with a normal contact force as constant as possible (2N). Under the assumption that the palm is fixed, the contact points can be estimated using joint encoder measurements and fingertip sensor readings. These contact positions are recorded and the contact point trajectory can be then used to deduce surface geometrical characteristics. In addition to the normal force, the tangential force is also recorded. When the velocity is not null but small, the dry friction coefficient is approximated by $k_{fr} = \frac{\|\boldsymbol{F}_t\|}{\|\boldsymbol{F}_n\|}$.

The results of the simulation test are shown in Fig. 18a. It was found that the normal force varied between 1.2 and 2.7 N during the simulation. For the experiments on the Shadow hand, the same procedure has been conducted: the palm is

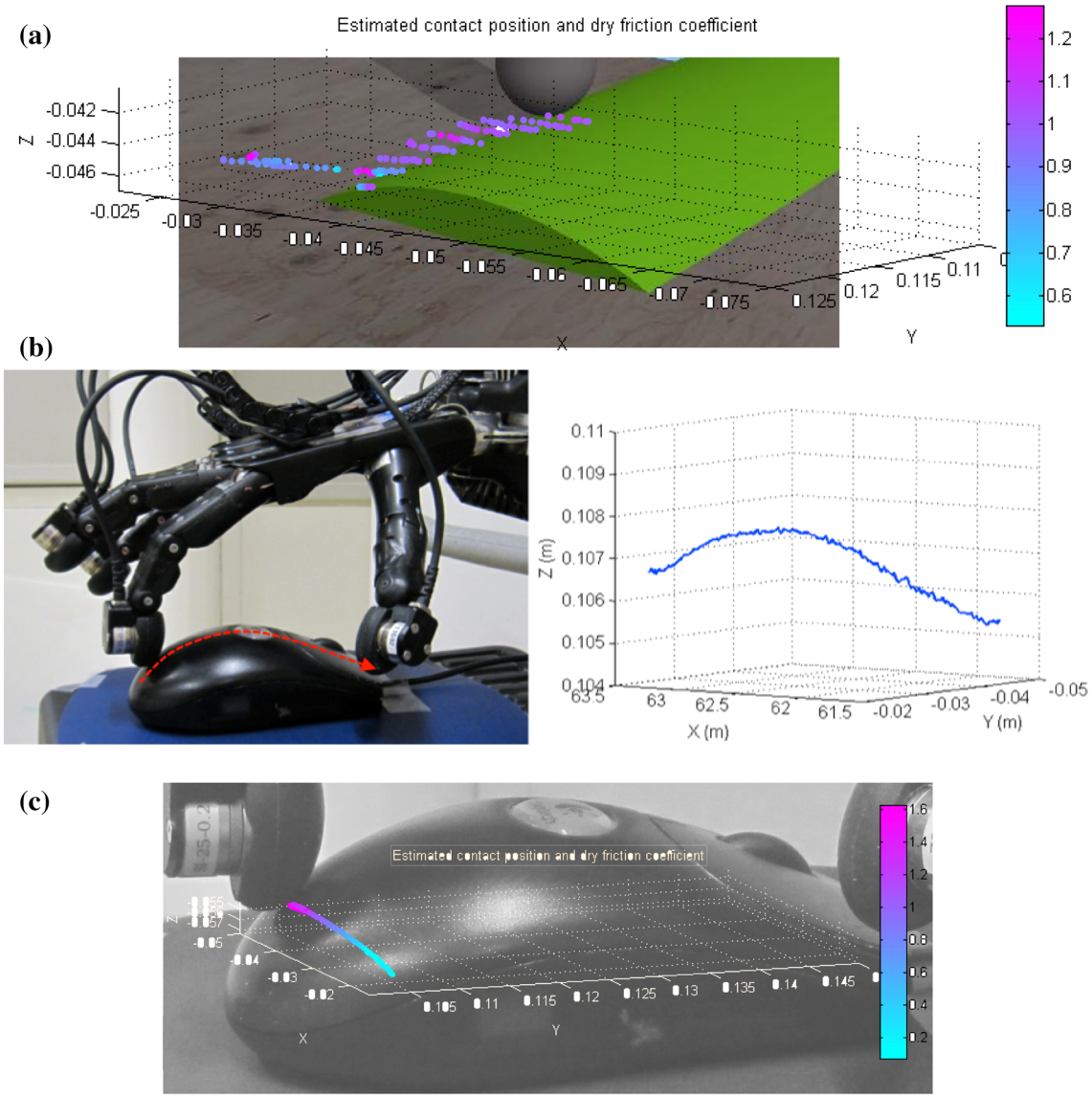

Fig. 18 Estimated contact position and dry friction coefficient k_{fr} (the value of the friction coefficient is given in colour scale). **a** shows the results from the simulation. **b** shows of results from a contour following experiment using the real hand (the *red dashed line* shows the real finger motion path and the 3D plot shows the identified contact trajectory of the finger motion). **c** shows the estimated friction coefficient k_{fr} using the Shadow^{TM} hand (Color figure online)

fixed to a laboratory frame; the fingertip is controlled to move from one point to others on an unknown surface, Fig. 18b. The desired contact normal force was set to 0.6 N for the real hand experiments. The reason of lowering the reference normal force from 2 to 0.6 N is to avoid the stick-slip phenomenon observed when sliding the rubber skin enveloping the finger onto a rigid object surface with a normal force ≈2 N. The contact trajectory and the dry friction coefficients are estimated using the same algorithm described above. The results of this experiment are shown in Fig. 18c. It was found that the normal force varied between 0.7 and 1.5 N during the test. These results are promising and show strong potential of using the contact-sensing fingertip in exploring object surface for the grasping and dexterous manipulation tasks. However it was also observed that the surface following control has issues regarding normal force control quality and target location reachability. One of the reasons may be due to the high friction coefficient k_{fr} between the rubber material and the object. It can be seen in Fig. 18 that $k_{fr} > 1.0$ at several places along the path. The high friction could result in inaccurate estimation of the surface normal as demonstrated in Sect. 4.3, thus impairing normal force control. In addition, the proposed surface following control assumes precise fingertip position control. Thus the error of finger position estimation due to the accumulated sensing errors of the finger joint angles could also deduct the control quality. An

in-depth analysis of the controller will be carried for future work.

6 Discussion and conclusion

This paper introduces a novel contact-sensing algorithm for a fingertip with deformable rubber skin equipped with a 6 axis force/torque sensor. Experimental studies demonstrate that the sensing algorithm is capable of providing accurate contact information along the whole surface of the fingertip at high speed with both large radius contact and small radius contact. There are few limitations associated with the current development of the contact-sensing fingertip. First, the relationship between the surface deformation and the normal reaction force is approximated using a single equation without considering surface geometry properties. Experiments show that this approximation works well when the normal force is below 6 N. However, in order to increase the working range of the fingertip, further analysis taking into account the surface geometry is required. In addition, a comparison study is required to evaluate the algorithm accuracy and computational efficiency with respect to different modelling techniques of soft material and numerical methods. This study will be carried out in the future work. Several studies are planned to be carried out in the future to improve the applicability of fingertip contact sensing method. Despite the promising results, the current surface following algorithm still presents some limitations. The first one concerns the magnitude of the normal force: to date, this normal force is still high ($\sim$1 N) during the exploration. This makes it difficult to explore light weight objects without moving them. One potential improvement is to make the fingertip force control more precise and rapid. The second issue is that this contour following controller searches for a local minimum only (closest point to the destination). Because of this, the finger could be trapped locally in some situations. In order to improve this, intermediate paths should be generated by a higher level program with the help of vision system or random search processes. Future work aims to improve the surface following control method to enable a dexterous hand equipped with the contact-sensing fingers to stably explore an unknown object and efficiently carry out fine in-hand manipulation.

Acknowledgments This research received support provided by the HANDLE project funded by the European Commission within the Seventh Framework Programme FP7 (FP7/2007-2013) under Grant Agreement ICT 231640.

References

Agache, P. G., Monneur, C., Leveque, J. L., & De Rigal, J. (1980). Mechanical properties and Young's modulus of human skin in vivo. *Archives of Dermatological Research*, *269*(3), 221–232.

Back, J., Bimbo, J., Noh, Y., Seneviratne, L. D., Althoefer, K., & Liu, H. (2014). Controlling a contact sensing finger for surface haptic exploration. In *IEEE International Conference on Robotics and Automation (ICRA)* (pp. 2736–2741).

Bard, Y. (1970). Comparison of gradient methods for the solution of nonlinear parameter estimation problems. *SIAM Journal on Numerical Analysis*, *7*(1), 157–186.

Bicchi, A., Salisbury, J. K., & Brock, D. L. (1993). Contact sensing from force measurements. *The International Journal of Robotics Research*, *12*(3), 249–262.

Bicchi, A. (2000). Hands for dexterous manipulation and robust grasping: A difficult road toward simplicity. *IEEE Transactions on Robotics and Automation*, *16*(6), 652–662.

Bimbo, J., Seneviratne, L. D., Althoefer, K., & Liu, H. (2013). Combining touch and vision for the estimation of an object's pose during manipulation. In *IEEE/RSJ International Conference on Intelligent Robots and Systems (IROS)* (pp. 4021–4026).

Bossert, D., Ly, U. L., & Vagners, J. (1996). Experimental evaluation of a hybrid position and force surface following algorithm for unknown surfaces. In *Proceedings of IEEE International Conference on Robotics and Automation*, 1996 (Vol. 3, pp. 2252–2257).

Chang, W. C. (2004). Cartesian-based planar contour following with automatic hybrid force and visual feedback. In *IEEE/RSJ International Conference on Intelligent Robots and Systems*, 2004 (Vol. 3, pp. 3062–3067).

Dahiya, R. S., Metta, G., Valle, M., & Sandini, G. (2010). Tactile sensing-from humans to humanoids. *IEEE Transactions on Robotics*, *26*(1), 1–20.

Dahiya, R. S., Cattin, D., Adami, A., Collini, C., Barboni, L., Valle, M., et al. (2011). Towards tactile sensing system on chip for robotic applications. *IEEE Sensors Journal*, *11*(12), 3216–3226.

Dargahi, J. (2000). A piezoelectric tactile sensor with three sensing elements for robotic, endoscopic and prosthetic applications. *Sensors and Actuators A: Physical*, *80*(1), 23–30.

De Maria, G., Natale, C., & Pirozzi, S. (2012). Force/tactile sensor for robotic applications. *Sensors and Actuators A: Physical*, *175*, 60–72.

De Maria, G., Natale, C., & Pirozzi, S. (2013). Tactile data modeling and interpretation for stable grasping and manipulation. *Robotics and Autonomous Systems*, *61*(9), 1008–1020.

Gálvez, J. A., & Gonzalez de Santos, P. (2001). Intrinsic tactile sensing for the optimization of force distribution in a pipe crawling robot. *IEEE/ASME Transactions on Mechatronics*, *6*(1), 26–35.

Ho, V. A., Dao, D. V., Sugiyama, S., & Hirai, S. (2011). Development and analysis of a sliding tactile soft fingertip embedded with a microforce/moment sensor. *IEEE Transactions on Robotics*, *27*(3), 411–424.

Howe, R. D., & Cutkosky, M. R. (1996). Practical force-motion models for sliding manipulation. *The International Journal of Robotics Research*, *15*(6), 557–572.

Inoue, T., & Hirai, S. (2006). Elastic model of deformable fingertip for soft-fingered manipulation. *IEEE Transactions on Robotics*, *22*(6), 1273–1279.

Inoue, T., & Hirai, S. (2009). *Mechanics and control of soft-fingered manipulation*. London: Springer.

Jamali, N., & Sammut, C. (2011). Majority voting: Material classification by tactile sensing using surface texture. *IEEE Transactions on Robotics*, *27*(3), 508–521.

Jatta, F., Legnani, G., & Visioli, A. (2006). Friction compensation in hybrid force/velocity control of industrial manipulators. *IEEE Transactions on Industrial Electronics*, *53*, 604–613.

Johansson, R. S., & Flanagan, J. R. (2009). Coding and use of tactile signals from the fingertips in object manipulation tasks. *Nature Reviews Neuroscience*, *10*(5), 345–359.

Kao, I., & Cutkosky, M. R. (1993). Comparison of theoretical and experimental force/motion trajectories for dextrous manipulation with

sliding. *The International Journal of Robotics Research*, *12*(6), 529–534.
Kao, I., & Yang, F. (2004). Stiffness and contact mechanics for soft fingers in grasping and manipulation. *IEEE Transactions on Robotics and Automation*, *20*(1), 132–135.
Kemp, C. C., Edsinger, A., & Torres-Jara, E. (2007). Challenges for robot manipulation in human environments [grand challenges of robotics]. *IEEE Robotics & Automation Magazine*, *14*(1), 20–29.
Lederman, S. J., & Klatzky, R. L. (1990). Haptic classification of common objects: Knowledge-driven exploration. *Cognitive Psychology*, *22*(4), 421–459.
Liang, X., & Boppart, S. A. (2010). Biomechanical properties of in vivo human skin from dynamic optical coherence elastography. *IEEE Transactions on Biomedical Engineering*, *57*(4), 953–959.
Liu, H., Song, X., Bimbo, J., Althoefer, K., & Seneviratne, L. (2012a). Surface material recognition through haptic exploration using an intelligent contact sensing finger. In *IEEE/RSJ International Conference Intelligent Robots and Systems* (pp. 52–57).
Liu, H., Song, X., Nanayakkara, T., Seneviratne, L. D., & Althoefer, K. (2012b). A computationally fast algorithm for local contact shape and pose classification using a tactile array sensor. In *IEEE International Conference on Robotics and Automation (ICRA)* (pp. 1410–1415).
Madsen, K., Nielsen, H. B., & Tingleff, O. (2004). *Methods for non-linear least square problems* (2nd ed.). IMM, DTU: Lecture Notes.
Murakami, K., & Hasegawa, T. (2005). Tactile sensing of edge direction of an object with a soft fingertip contact. In *Proceedings of the 2005 IEEE International Conference on Robotics and Automation* (pp. 2571–2577).
Nguyen, K. C., & Perdereau, V. (2013). Fingertip force control based on max torque adjustment for dexterous manipulation of an anthropomorphic hand. In *IEEE/RSJ International Conference on Intelligent Robots and Systems (IROS)* (pp. 3557–3563).
Ohka, M., Kobayashi, H., Takata, J., & Mitsuya, Y. (2008). An experimental optical three-axis tactile sensor featured with hemispherical surface. *Journal of Advanced Mechanical Design, Systems, and Manufacturing*, *2*(5), 860–873.
Okamura, A. M., & Cutkosky, M. R. (2001). Feature detection for haptic exploration with robotic fingers. *The International Journal of Robotics Research*, *20*(12), 925–938.
Olsson, H., Åström, K. J., Gäfvert, M., & Lischinsky, P. (1998). Friction models and friction compensation. *European Journal of Control*, *4*(3), 176–195.
Pawluk, D. T., & Howe, R. D. (1999). Dynamic lumped element response of the human fingerpad. *Journal of Biomechanical Engineering*, *121*(2), 178–183.
Puangmali, P., Liu, H., Seneviratne, L. D., Dasgupta, P., & Althoefer, K. (2012). Miniature 3-axis distal force sensor for minimally invasive surgical palpation. *IEEE/ASME Transactions on Mechatronics*, *17*(4), 646–656.
Rothwell, J. C., Traub, M. M., Day, B. L., Obeso, J. A., Thomas, P. K., & Marsden, C. D. (1982). Manual motor performance in a deafferented man. *Brain*, *105*(3), 515–542.
Salisbury, J. Jr. (1984). Interpretation of contact geometries from force measurements. In *Proceedings of the IEEE International Conference on Robotics and Automation*, 1984 (Vol. 1, pp. 240–247). IEEE.
Salo, T., Vančura, T., & Baltes, H. (2006). CMOS-sealed membrane capacitors for medical tactile sensors. *Journal of Micromechanics and Microengineering*, *16*(4), 769–778.
Schmitz, A., Maiolino, P., Maggiali, M., Natale, L., Cannata, G., & Metta, G. (2011). Methods and technologies for the implementation of large-scale robot tactile sensors. *IEEE Transactions on Robotics*, *27*(3), 389–400.
Shimojo, M., Namiki, A., Ishikawa, M., Makino, R., & Mabuchi, K. (2004). A tactile sensor sheet using pressure conductive rubber with electrical-wires stitched method. *IEEE Sensors Journal*, *4*(5), 589–596.
Song, X., Liu, H., Bimbo, J., Althoefer, K., & Seneviratne, L. D. (2012). A novel dynamic slip prediction and compensation approach based on haptic surface exploration. In *IEEE/RSJ International Conference on Intelligent Robots and Systems (IROS)* (pp. 4511–4516).
Song, X., Liu, H., Althoefer, K., Nanayakkara, T., & Seneviratne, L. D. (2014). Efficient break-away friction ratio and slip prediction based on haptic surface exploration. *IEEE Transactions on Robotics*, *30*(1), 203–219.
Teshigawara, S., Tsutsumi, T., Shimizu, S., Suzuki, Y., Ming, A., Ishikawa, M., & Shimojo, M. (2011). Highly sensitive sensor for detection of initial slip and its application in a multi-fingered robot hand. In *IEEE International Conference on Robotics and Automation (ICRA)* (pp. 1097–1102).
Wettels, N., Santos, V. J., Johansson, R. S., & Loeb, G. E. (2008). Biomimetic tactile sensor array. *Advanced Robotics*, *22*(8), 829–849.
Wisitsoraat, A., Patthanasetakul, V., Lomas, T., & Tuantranont, A. (2007). Low cost thin film based piezoresistive MEMS tactile sensor. *Sensors and Actuators A: Physical*, *139*(1), 17–22.
Xydas, N., & Kao, I. (1999). Modeling of contact mechanics and friction limit surfaces for soft fingers in robotics, with experimental results. *The International Journal of Robotics Research*, *18*(9), 941–950.
Yamada, T., Tanaka, A., Yamada, M., Yamamoto, & H., Funahashi, Y. (2010). Autonomous sensing strategy for parameter identification of contact conditions by active force sensing. In *IEEE International Conference on Robotics and Biomimetics (ROBIO)* (pp. 839–844).
Yousef, H., Boukallel, M., & Althoefer, K. (2011). Tactile sensing for dexterous in-hand manipulation in robotics–A review. *Sensors and Actuators A: Physical*, *167*(2), 171–187.

Hongbin Liu is currently a Lecturer (Assistant Professor) in the Department of Informatics, King's College London, UK. He received the B.S. degree in 2005 from the Northwestern Polytechnique University, Xi'an, China, awarded the M.Sc. degree from King's College London in 2006. He received the Ph.D. degree in 2010 from Kings College London. He is a member of IEEE. His research interests include the tactile/force perception based robotic cognition, the modelling of dynamic interaction, medical robotics and haptics.

Kien Cuong Nguyen received the MS degree in robotics, automatics and vision from Ecole Polytechnique and Ecole des Mines de Paris in 2009. He is currently working toward the Ph.D. degree with the Institut des Systèmes Intelligents et de Robotique, Université Pierre et Marie Curie (UPMC), Paris. His main research interests include the applications of biological-inspired mechanisms to robotics. His current research is mainly focused on grasping and dexterous manipulation of an anthropomorphic hand.

Véronique Perdereau is full Professor at Université Pierre et Marie Curie (UPMC) since 2003 and recognized as a IEEE senior member since 2001. She obtained her Electrical and Information Engineering MS in 1987 and Robotics and Automation Ph.D. degree in 1991. She is Assistant Professor at UPMC since 1987 and Ph.D. advisor since 2000, full Professor since 2003, chair of the IEEE Education France chapter. Her main research interests include hybrid position/force control and vision based control of robot manipulators.

Joao Bimbo is currently a PhD student in the Centre for Robotics Research at King's College London. He obtained M.Sc. degree in Electrical and Computer Engineering from the University of Coimbra, Portugal in 2011. He started his Ph.D. studies in October 2011 in the field of sensing for robot grasping. His research interests include fusion of tactile and vision for grasping and estimation of object's physical properties.

Junghwan Back is currently a Ph.D. student in the Centre for Robotics Research at King's College London. He obtained M.Sc. degree in Robotics from King's College London in 2013. He started his Ph.D. studies in January 2014 in the field of force control for deformable contact. His research interests include adaptive force control, modelling of the continuum robot and tactile sensing.

Matthew Godden is Senior Robotics Design Engineer at Shadow Robot Company, where he has worked on each of the eight generations of Shadow Dexterous Hands both Air Muscle and electric motor driven. He is experienced in both design and application of Air Muscles (a novel pneumatic actuator) and has designed and developed several devices that interact with humans directly and safely including a 7 meter long 6DoF interactive limb as a dance partner called Spidercrab.

Lakmal D. Seneviratne received the B.Sc. (Eng.) and Ph.D. degrees in mechanical engineering from King's College London (KCL), London, UK, in 1980 and 1985, respectively. He is currently a Professor of Robotics at Khalifa University, Abu Dhabi, UAE, on secondment from KCL, where he is a Professor of mechatronics. He has published over 250 refereed research papers related to robotics and mechatronics. His research interests include robotics and intelligent autonomous systems. Prof. Seneviratne is a Fellow of the Institution of Engineering (IET) and Technology and the Institution of Mechanical Engineers (IMechE).

Kaspar Althoefer received the Dipl.-Ing. degree in electronic engineering from the University of Aachen, Aachen, Germany, and the Ph.D. degree in electronic engineering from King's College London, London, UK. He is currently a Professor of Robotics and Intelligent Systems and Head of the Centre for Robotics Research (CoRe), Department of Informatics, King's College London. He has been involved in research on mechatronics since 1992 and gained considerable expertise in the areas of sensing, sensor signal analysis, embedded intelligence, and sensor data interpretation as well as robot-based applications. He has authored or coauthored more than 180 refereed research papers related to mechatronics and robotics.